A NEW METHOD FOR OBTAINING ISOPACHIC PATTERNS

by

JAMES REVELL KIMZEY
B. S., M. E., University of Arkansas, 1961

A MASTER'S REPORT

submitted in partial fulfillment of the

requirements for the degree

MASTER OF SCIENCE

Department of Applied Mechanics

KANSAS STATE UNIVERSITY
Manhattan, Kansas

1963

Approved by:

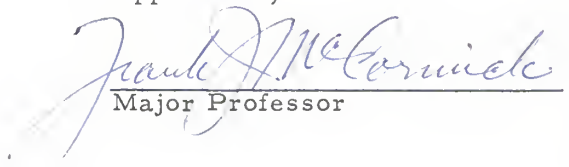

Major Professor

TABLE OF CONTENTS

NOMENCLATURE

a	amplitude of light ray
T	time
ω	circular frequency
Ψ	angle between polarizer axis and directions of principal stresses
R	wavelengths of relative retardation
t	model thickness
C	stress optical coefficient of birefringent material
σ_1	maximum principal stress
σ_2	minimum principal stress
τ	shearing stress
ρ	radius of curvature of stress trajectory
s	distance measured along a stress trajectory
Σ	sum of the principal stresses, i.e., $(\sigma_1 + \sigma_2)$
ϵ	strain
ν	Poisson's ratio
E	modulus of elasticity
∇^2	Laplacian operator
δ	mesh spacing
λ	wavelength of light
μ	absolute index of refraction
L	physical path length of light
ϕ	angle of incidence
α	angle of refraction

NOMENCLATURE concl.

I	intensity of light source
ΔN	isopachic fringe order
K	isopachic calibration constant

INTRODUCTION

Effective methods of determining isopachic patterns in plane stress structures and models have been eagerly sought for the last half century. The isopachic pattern describes the thickness changes caused by loading a two-dimensional model and therefore represents the sum of the principal stresses at all points of the plane stress systems. When used in conjunction with the conventional isochromatic pattern of photoelasticity, which represents the difference of the principal stresses at all points in a model, simple evaluation or separation of the individual principal stresses is made possible.

Numerous instruments for measuring minute thickness changes have been devised (3). The earliest ones were sensitive, delicate instruments capable only of point by point scanning of models under investigation. Instruments and techniques for observing isopachics over large fields are fewer in number. These are elaborate, expensive instruments, and highly sensitive to external vibrations and temperature changes. None has been successful enough to replace the laborious and time-consuming integration and iteration procedures of conventional photoelasticity.

The purpose of this paper is to present a new method for obtaining isopachic patterns which is a significant improvement over the methods now available.

PHOTOELASTIC TECHNIQUE

An understanding of the photoelastic technique is necessary if a comparison of the methods of separating the principal stresses is to be made.

Examining the effect of a homogenous plate of doubly refracting material upon a normal beam of monochromatic, plane polarized light, as shown in Fig. 1, it is seen that the plane polarized beam represented by the vector $A = a \sin \omega t$ is resolved into two components along the optical axes of the plate. Due to the property of double refraction the light travels through the plate faster along one of the optical axes than the other. Upon passing through the analyzer the emergent components are reduced to the vector A':

$$A' = (a \sin 2\Psi)(\sin \pi R)(\cos(\omega T + 2\pi R) \qquad (1a)$$

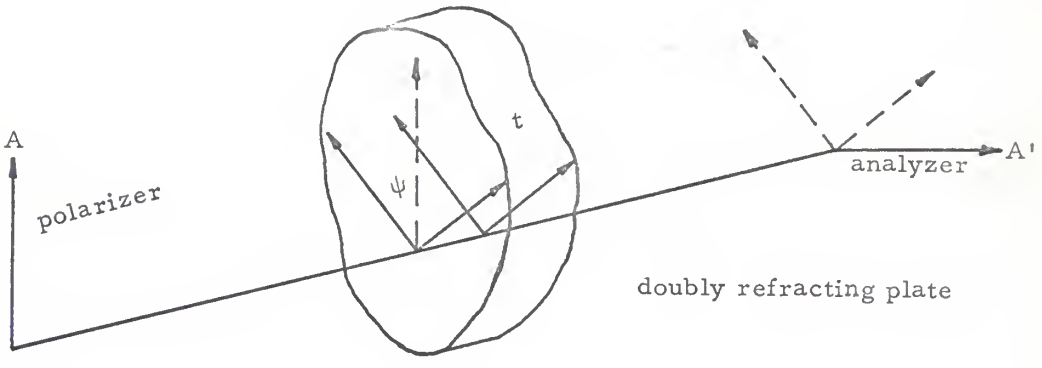

Fig. 1. Doubly refracting plate.

in which R represents the phase difference developed as a result of the different transmission velocities along the optical axes of the doubly refracting medium.

In 1816, Sir David Brewster discovered that certain isotropic transparent materials are made artificially doubly refracting by applied stresses. Photoelasticians call the property of double refraction "birefringence."

In 1852, Maxwell formulated the following laws:

(1) At any point in a birefrigent material the optical axes of double refraction are parallel to the direction of the principal stresses.

(2) The phase different developed by a two-dimensional stress system in a birefringent material is given by $R = Ct(\sigma_1 - \sigma_2)$.

The second law requires that the stresses be within the elastic limit.

Using the second law formulated by Maxwell it is seen that the light passed by the analyzer is given by

$$A' = a \sin 2\Psi \sin(\pi Ct(\sigma_1 - \sigma_2)\cos(\omega T + 2\pi R) \qquad (1b)$$

The amplitude of A' is then

$$a \sin 2\Psi \sin(\pi Ct(\sigma_1 - \sigma_2)) = a \sin 2\Psi \sin \pi R \qquad (1c)$$

Since the intensity is proportional to the square of the amplitude it will be a minimum under the following two conditions:

(1) $\Psi = \frac{n\pi}{2}$ $\qquad n = 0, 1, 2, 3 \ldots$

(2) $R = m = Ct(\sigma_1 - \sigma_2)$ $\qquad m = 0, 1, 2, 3 \ldots$

From the first of these conditions and Maxwell's first law it can be deduced that the principal stresses in the stressed plate of birefringent material are parallel to the polarizer and analyzer, respectively. At all points at which this occurs the intensity of light transmitted by the analyzer will be zero, regardless of the wavelength and the magnitude of $\sigma_1 - \sigma_2$. If then the stressed birefringent material be viewed through the analyzer, certain black regions will be observed showing the locus of all points at which the directions of principal stress are parallel to the axes of the polarizer and analyzer. These black regions are called isoclinic lines or fringes, or simply isoclinics. An isoclinic then is the locus of points along which the principal stresses have parallel directions. In general, the directions of the principal stresses will vary from point to point in the loaded plate, so that if the polarizer and analyzer are rotated together, the isoclinics will move to points of the plate at which the principal stresses are parallel to the new directions of the polarizing axes of the analyzer and polarizer. Thus different sets of isoclinic lines are obtained for different orientations of polarizer and analyzer. It is usual to take as standard directions the vertical and horizontal and to measure the inclinations of the principal stresses counter-clockwise from these directions. Then for an n^o inclination of the polarizer a set of fringes is obtained which is called the n^o isoclinics along which the principal stresses in the plane of the plate are inclined n^o to the vertical and horizontal.

It should be noted that in regions where the directions of the principal stresses are changing very slowly from point to point the intensity of light passed by the analyzer will be changing slowly. In such regions then, the isoclinics will appear as poorly defined, diffuse dark fringes. The true isoclinics in such a case are the lines of least illumination and must be judged by eye.

The second condition for zero intensity is that $R = m$. If then the loaded plate is viewed through the analyzer, dark regions will appear at points where the relative retardation is zero or an integral number of wavelengths. Along these lines the principal stress difference $\sigma_1 - \sigma_2 = m/tC$ is constant. Such lines are called isochromatic fringes or simply isochromatics. Then each integral value of m will yield a dark line, if the loaded plate is viewed through the analyzer, along which $\tau_{max} = \frac{\sigma_1 - \sigma_2}{2} = \frac{m}{2tC}$ is constant. In effect, the diameter of Mohr's circle has been determined. The integer m is called the fringe order and the constant $1/tC = F$ is called the model fringe value, while the constant $1/C$ is called the material fringe value. These constants are usually determined experimentally.

By suitable optical arrangements the two effects $\Psi = n\pi/2$ and $R = m$ can be obtained separately and thus the directions of the principal stresses and their difference throughout the stressed birefringent material determined independently. The isoclinics and isochromatics shall hereafter be referred to as photoelastic data.

If a two-dimensional stress system is to be investigated then the procedure is to form a model in the shape desired from some birefringent material of constant thickness and load it under the elastic limit with the two-dimensional load distribution under investigation. The direction of the principal stresses and their difference can then be determined as outlined above.

Equations of Elasticity

The usual object of an experimental stress analysis is to obtain the individual principal stresses and the directions at which they act. To achieve this end through the photoelastic technique, the theory of elasticity must be utilized. The discussion will be limited to the state of plane stress: $\sigma_z = 0$.

Considering the equilibrium of a small rectangular element subjected to a two-dimensional stress system and neglecting body forces, such as inertia, the equations of equilibrium in Cartesian coordinates are found by force summations in the coordinate directions to be

$$\frac{\partial \sigma_x}{\partial x} + \frac{\partial \tau_{xy}}{\partial y} = 0 \tag{2}$$

and

$$\frac{\partial \sigma_y}{\partial y} + \frac{\partial \tau_{xy}}{\partial x} = 0. \tag{3}$$

It should be noted that the omission of body forces limits these equations to the case of static equilibrium.

Considering the equilibrium of a curvilinear rectangle, formed by intersecting stress trajectories, the equations of equilibrium in

curvilinear coordinates are obtained. These equations are called the Lame'-Maxwell equations of equilibrium. They are

$$\frac{\partial \sigma_1}{\partial s_1} + \frac{\sigma_1 - \sigma_2}{\rho_2} = 0 \tag{4}$$

and

$$\frac{\partial \sigma_2}{\partial s_2} + \frac{\sigma_1 - \sigma_2}{\rho_1} = 0. \tag{5}$$

Stress trajectories are lines to which the principal stresses are tangent at all points and are obtained by graphical construction from the isoclinics.

In two dimensions the equations of compatibility reduce to a single equation. This equation for the state of plane stress, neglecting body forces as before, may be written in terms of the stresses as

$$\left[\frac{\partial^2}{\partial x^2} + \frac{\partial^2}{\partial y^2}\right](\sigma_x + \sigma_y) = 0. \tag{6}$$

Remembering that the sum of the normal stresses at a point is constant, i.e., $\sigma_x + \sigma_y = \sigma_1 + \sigma_2$, it is seen that the sum of the principal stresses satisfies Laplace's equation in two dimensions.

Hooke's law gives the strain in the transverse direction as

$$\epsilon_z = \frac{1}{E}\left(\sigma_z - \nu(\sigma_x + \sigma_y)\right). \tag{7}$$

This equation reduces to

$$\epsilon_z = -\frac{\nu}{E}(\sigma_1 + \sigma_2) \tag{8}$$

since the sum of the normal stresses at a point is constant. It may be noted also that $\tau_{xy} = \frac{\sigma_1 - \sigma_2}{2} \sin 2\theta$ where θ is the angle measured from the axis to the direction of maximum principal stress.

Separation of the Principal Stresses by Conventional Methods

Returning to the problem of analyzing photoelastic data, i.e., separating the principal stresses, several established methods are available using the photoelastic data in conjunction with the results of the theory of elasticity. The method employed necessarily depends upon the particular problem involved, the accuracy desired, and the equipment and time available. All the methods, however, can be categorized under the following headings:

(A) Integration of the equations of equilibrium

(B) Determination of the sum of the principal stresses

(1) Numerical solution of Laplace's equation

(2) Experimental methods.

Integration of the Equations of Equilibrium. Considering the integration of the equations of equilibrium, the general procedure in rectangular co-ordinates is to construct a normal to a free boundary and label this normal as either the x or y axis, as shown in Fig. 2. The appropriate equation of equilibrium is then integrated along this normal. Using Eq. (2) and integrating from x_o to x_1:

$$\int_{x_0}^{x_1} \frac{\partial \sigma_x}{\partial x} dx + \int_{x_0}^{x_1} \frac{\partial \tau_{xy}}{\partial y} dx = \sigma_x \Big|_{x_1} - \sigma_x \Big|_{x_0} + \int_{x_0}^{x_1} \frac{\partial \tau_{xy}}{\partial y} dx = 0. \tag{9}$$

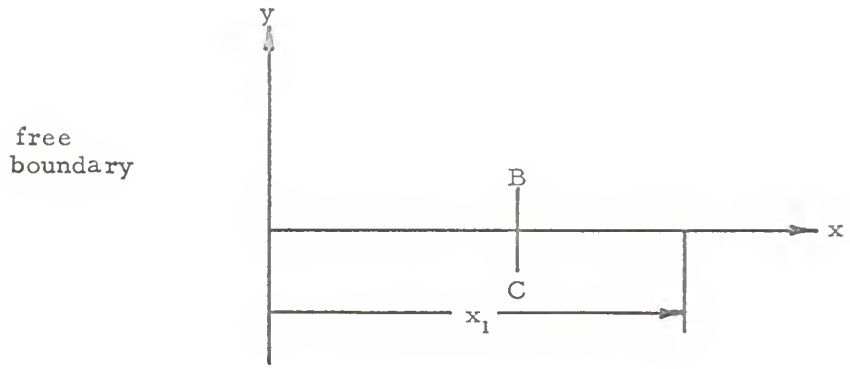

Fig. 2. Normal to free boundary.

Since the point x_0 is on the free boundary, one of the principal stresses must be zero there. The isochromatic fringe pattern then yields directly the principal stress at that point. The direction of this principal stress may be obtained from the isoclinics. Mohr's circle can then be used to determine $\sigma_x \Big|_{x_1}$. The problem of evaluating $\int_{x_0}^{x_1} \frac{\partial \tau_{xy}}{\partial y} dx$ remains, however, if $\sigma_x \Big|_{x_1}$ is to be found. From the theory of elasticity $\tau_{xy} = \frac{\sigma_1 - \sigma_2}{2} \sin 2\theta$. The isochromatic pattern yields $(\sigma_1 - \sigma_2)$ while the angle θ is obtained from the isoclinics. Therefore τ_{xy} may be evaluated.

If the shearing stress is then plotted as a function of the co-ordinate y at intervals along the x axis, its slope, i.e., $\frac{\partial \tau_{xy}}{\partial y}$, may be determined graphically at each such point and a plot of $\frac{\partial \tau_{xy}}{\partial y}$ as a function of x obtained. Graphical integration

of this plot then yields the desired integral. If the shear stress is not changing too rapidly, a quicker method of determining $\frac{\partial \tau_{xy}}{\partial y}$ is simply to evaluate τ_{xy} at two points, B and C, near to one another, and then divide the difference between these values by the length BC. This scheme is called the shear difference method and is attributed to Frocht (3).

The integration of the Lame'- Maxwell equations of equilibrium along a stress trajectory follows the same general procedure.

Determination of the Sum of the Principal Stresses. If the sum of the principal stresses can be found, a complete solution of the photoelastic problem is obtained. The isochromatic pattern yields the difference of the principal stresses so addition and subtraction with the sum gives the individual principal stresses, i. e., separates them.

Numerical Solution of Laplace's Equation. The sum of the principal stresses is a harmonic function. All harmonic functions possess one fundamental property that is formulated in Dirichlet's theorem. This theorem states that for a given boundary Γ surrounding a region R to which the function applies, and for specified boundary values on Γ, there exists only one solution of Laplace's equation for all points within the region R. It follows that the sum of the principal stresses is uniquely determined at every point within a given region of a two-dimensionally stressed body provided the boundary stresses are known.

It will be recalled that the photoelastic technique yields Σ on the free boundaries in that $\sigma_1 - \sigma_2$ is obtained from the isochromatics, and one of the principal stresses must be zero on a free boundary. Numerical techniques for solving $\nabla^2 \Sigma$ utilizing these boundary stresses would then yield a unique solution for Σ in the interior of the stressed body.

There are several techniques used to carry out the numerical solution desired, including the methods of algebraic harmonization, iteration, the linear rosette method, block iteration, method of differences, and the relaxation method. Each varies in complexity, accuracy, and time involved. The relaxation method will be examined briefly, in order to illuminate the general procedures involved and some of the difficulties that may be encountered.

Consider the region for which Σ is defined divided into a gridwork as shown in Fig. 3. Approximating Laplace's equation by means of the divided differences $\frac{\partial^2 \Sigma}{\partial y^2} \cong \frac{\Sigma_2 - 2\Sigma_0 + \Sigma_4}{\delta^2}$ and $\frac{\partial^2 \Sigma}{\partial x^2} \cong \frac{\Sigma_1 - 2\Sigma_0 + \Sigma_3}{\delta^2}$ substitution leads to

$$\Sigma_0 = \frac{\Sigma_1 + \Sigma_2 + \Sigma_3 + \Sigma_4}{4} . \qquad (10)$$

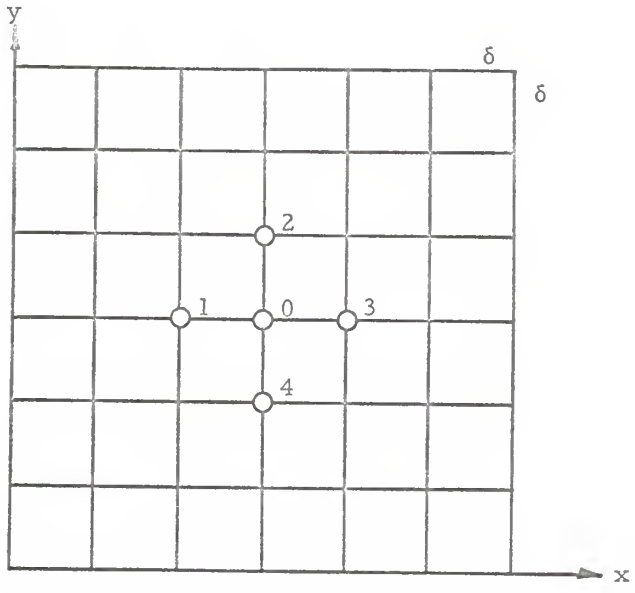

Fig. 3. Relaxation method network.

In the interior of the region in question, values for Σ are assumed at each nodal point of the constructed network. Starting at the boundary points where the correct values of Σ are known from the isochromatics, a traverse of the network is made calculating new values for Σ at the nodal points using Eq. (10). These values will be different from the ones assumed in that they are influenced by the correct values on the boundaries. The process is repeated until the interior values become stationary.

Experimental Methods. Historically, the experimental determination of Σ was the first method employed to separate the principal stresses. It is a direct application of Hooke's law for the state of plane

stress, that is

$$\epsilon_z = \frac{-\nu}{E}(\sigma_1 \quad \sigma_2) = \frac{\Delta t}{t} \quad . \tag{11}$$

Solving for Σ gives

$$\sigma_1 + \sigma_2 = \left(\frac{-E}{t\nu}\right)\Delta t. \tag{12}$$

in which Δt denotes the change in thickness. Now if the changes in thickness at the point in question can be measured with sufficient accuracy a complete solution of the photoelastic problem is obtained, in that the sum and difference of the principal stresses will be known. The instruments used to determine Δt are called lateral extensometers, and may be classified generally as mechanical, electrical, or optical.

In order to gauge the efficiency of this method an estimate of the order of displacements to be measured is desirable. Modern birefringent materials will produce observable relative retardations of approximately 1/20 of a wavelength. This corresponds to a $5/t$ lb/in.^{2} stress difference. Applying this to a typical birefringent tension test specimen it is seen that this produces a change in thickness of $5(10^{-6})$ in.

Obviously, lateral extensometers must be quite sensitive if the data obtained with them is to compare with that obtained from the isochromatic pattern.

Coker (1), one of the founders of the photoelastic method, employed a mechanical lateral extensometer in his pioneering work. It was a caliper-type device utilizing levers to amplify the effect and was necessarily adaptable only to point by point measurements.

A. V. de Forest and A. R. Anderson (2) developed a caliper type device utilizing resistance strain gages so arranged as to give the desired magnification. Again this was a point by point measuring device thereby making the determination of Σ over a large region of interest laborious.

The optical lateral extensometers are all interferometers. Most are of the simple two-beam type which employ division of amplitude as compared to division of wave front.

Consider a beam of monochromatic light of wave length λ meeting the surface of a plane parallel transparent plate of thickness t and refractive index μ, as shown in Fig. 4.

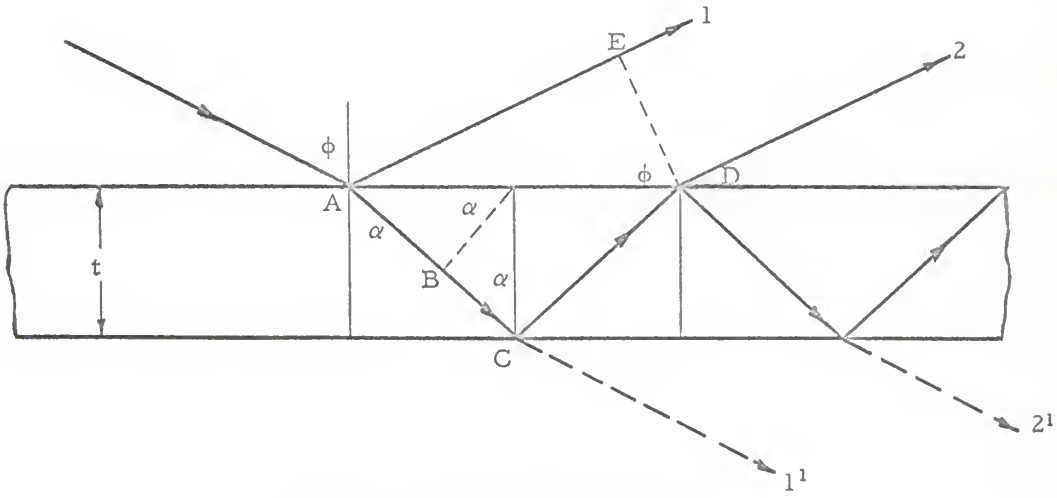

Fig. 4. Two beam interference.

Part of the beam is reflected as ray 1, and the remainder refracts to C at which point it is partially reflected to D. At D partial reflection takes place again and ray 2 emerges. The distances from the eye are so large in comparison with the thickness that rays 1 and 2 may

be considered to be essentially parallel. The distances from E and D to the eye are then equal. Rays 1 and 2 will then interfere constructively or destructively, depending on the phase difference developed by their different paths to the eye from the point of incidence A.

The optical path length is defined as $\sum_i \mu_i L_i$ where μ_i is the absolute refractive index and L_i is the physical path length of the medium through which the light ray is passing.

Snell's law for rays passing from one medium to another states that $\mu_1 \sin \phi_1 = \mu_2 \sin \alpha_2$ where μ_1 and μ_2 are the absolute indices of refraction of the media, and ϕ_1 and α_2 are the angles of incidence and refraction of the respective media.

The physical path length of ray 1 is AE = AD sin ϕ. Hence its optical path length is AD sin ϕ since the absolute index of refraction of air is unity.

The physical path length of ray 2 is

$$2AC = 2 \quad AD + BC \quad = 2\left(\frac{AD}{2} \sin \alpha + t \cos \alpha\right) \tag{13}$$

The optical path length is then

$$\mu \ AD \sin \alpha \ + \ 2\mu t \cos \alpha \tag{14}$$

By Snell's law $\sin \phi = \mu \sin \alpha$ so the optical path of ray 2 can then be written as

$$AD \sin \phi \ + \ 2\mu t \cos \alpha \tag{15}$$

The optical path difference then is $2\mu t \cos \alpha$ where α is the angle of refraction. Including a retardation of $\lambda/2$ of ray 1 upon reflection from a denser medium to air it is seen that destructive interference could occur when the optical path difference is an integral number of wavelengths and constructive interference could occur when the difference is equal to an odd number

of half wavelengths.

$$N\lambda = 2\mu t \cos\alpha \text{ -- possible destructive interference} \quad (16)$$

$$(N + 1/2)\lambda = 2\mu t \cos\alpha \text{ -- possible constructive interference} \quad (17)$$

$$N = 1, 2, 3, \ldots$$

For normal incidence, $\alpha = 0$, and these relations become

$$N\lambda = 2\mu t \quad (18)$$

$$(N + 1/2)\lambda = 2\mu t \quad (19)$$

The intensities of the reflected rays 1 and 2 must be examined to determine whether interference to an observable degree will in fact occur. Taking the plate material to be glass or plastic which have reflectivities of approximately 4 per cent and the intensity of the impingent ray to be I, it is seen that the intensity of ray 1 is 0.04 I, and that of ray AB is 0.96 I. After partial reflection at C ray DC will have intensity (0.04) (0.96 I). Finally, the partial reflectionat D gives the intensity of ray 2 as (0.04)(0.96 I) (0.96) = 0.037 I. The intensities and therefore the amplitudes of rays I and 2 are almost the same so observable interference can in fact occur. Examining the intensities of ray 1' and 2', it is seen that their intensities are 0.9216 I and 0.0147 I, respectively, so the transmitted light will not produce observable interference unless partially reflecting coatings are applied to the surfaces of the sheet material.

For normal incidence, the fringes appear localized at the surface of the plate.

If a wedge of quite small angle is considered, as shown in Fig. 5, the basic relation for normal incidence $N\lambda = 2\mu t$ holds closely enough. The possible variables are N, λ, μ, and t.

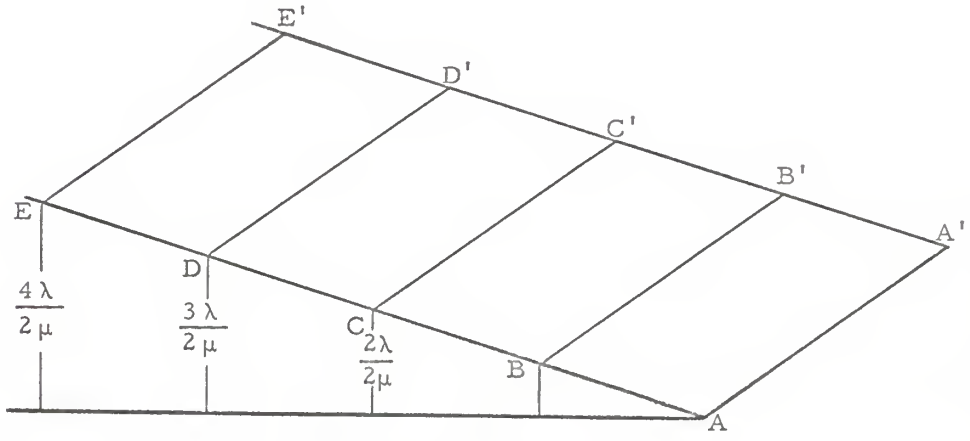

Fig. 5. Wedge fringes.

Using monochromatic light and materials with constant indices of refraction the variables reduce to N and t. Then the locus of points that satisfy Eq. (18) form dark bands or interference fringes representing lines of constant plate thickness. Adjacent fringes indicate thickness variations of $\lambda/2\mu$. In Fig. 5, then the lines BB', CC', etc., are called "fringes of equal thickness" and each fringe is a traverse of points for which the wedge thickness is constant. The fringes can be considered as height contour lines exactly as on a geographical contour map. If either of the two surfaces is irregular, then the fringes will be the map of the irregularities, each following a path of constant thickness. If the plate is initially optically flat no

fringe patterns will be observed. On the other hand the plate may display extreme thickness variations in which case the fringes are so densely spaced that they become indistinguishable.

If an originally optically flat model is loaded two dimensionally, thickness variations occur which are proportional to $(\sigma_1 + \sigma_2)$ since $\Delta t = -\frac{\nu t}{E}(\sigma_1 + \sigma_2)$. The appearing fringes will then give directly the loci of points along which the thickness changes between the strained and unstrained state is constant and therefore the loci of points along which $(\sigma_1 + \sigma_2)$ is constant. Such fringes are called isopachic fringes. The term isopachic is due to Coker and Filon (1) and is derived from the Greek words iso, meaning same, and pachic, meaning thickness.

The Mach-Zehnder and Michelson interferometers may be adapted for the determination of isopachic patterns using models which are initially optically flat. These are elaborate and very expensive instruments and are highly sensitive to vibration and temperature changes.

Frocht (3) observed the interference of light from the surfaces of a model originally optically flat and an auxiliary optical flat placed close to the model.

SUMMARY OF CONVENTIONAL METHODS

The integration of the equations of equilibrium in Cartesian coordinates involves the graphical evaluation of $\frac{\partial \tau_{xy}}{\partial y}$ and of the integral $\int_{x_0}^{x_1} \frac{\partial \tau_{xy}}{\partial y}\, dx$. Hence errors due to this graphical

evaluation are bound to arise in the solution. Experience aids in reducing such errors but regardless of the care exercised, the experimental error involved is difficult to determine. Note also that this method utilizes the isoclinics which may be inaccurate as implied previously. If the region of interest is remote from a free boundary, this method is quite time-consuming.

Integration of the Lame'-Maxwell equations of equilibrium along a stress trajectory is also subject to the errors inherent in a graphical evaluation, in that the stress trajectories and radii of curvature must be determined graphically. The use of the isoclinic patterns in determining the stress trajectories introduces further inaccuracies. Filon (1) and Frocht (3) have set forth methods by which these inherent errors may be reduced but their methods are only applicable to special types of problems.

The accuracy of the relaxation method obviously depends upon the mesh of the constructed gridwork and the number of traverses carried out. It is time-consuming if the assumed initial values in the interior are very much different from the correct ones. However, in regions where the isoclinics cannot be found with sufficient accuracy to utilize the shear difference method, it is decidedly useful

The determination of isopachic patterns by the usual interferometric means is an expensive operation in that equipment costs become prohibitive. The requirement that the model be originally optically flat is rather stringent for the ordinary photoelastic laboratory.

A NEW METHOD FOR OBTAINING ISOPACHIC PATTERNS

The classical optical methods for obtaining the sum of the principal stresses require that the model be initially optically flat.

If, however, a model that is not optically flat, but one that exhibits only slight thickness variations in the unstrained state is used, many of the difficulties mentioned above may be eliminated: Such a model would display fine, sparsely spaced thickness contour interference fringes satisfying $N\lambda = 2\mu t$ under monochromatic normally incident light. Under loading these fringes would move to new locations as a result of the thickness changes produced. The number of fringes passing a point would be directly proportional to the thickness change at that point. If the model were observed under loading and the fringes passing the point counted, the sum of the principal stresses could be found.

Considering a point in the model in both the unstrained and strained states, it is seen that the thickness contour or interference fringes at that point satisfy the relations $N\lambda = 2\mu t$ and $N'\lambda = 2\mu t'$ before and after loading. The thickness change then is

$$\Delta t = \frac{\lambda}{2\mu}(N' - N) = \Delta N \frac{\lambda}{2\mu} \tag{20}$$

ΔN is called the relative fringe order, the fringe shift, or simply the isopachic fringe order and is the number of fringes passing the point in question as mentioned above. Now

$$\frac{\Delta t}{t} = \Delta N \frac{\lambda}{2 \mu t} = - \frac{\nu}{E} (\sigma_1 + \sigma_2) = \epsilon_z \qquad (21)$$

from Eqs. (11) and (20).

Solving for Σ gives

$$\sigma_1 + \sigma_2 = \frac{-\lambda E}{2 \mu \nu t} (\Delta N) = - \frac{K}{t} \Delta N \qquad (22)$$

The constant K is called the isopachic calibration constant and may be determined by substituting the appropriate values or by experimentation.

Instead of observing the region of interest point by point under loading and counting the number of fringes which move past, photographs of the model in the unstrained and strained states may be taken. Starting at a point of known or zero Σ on the photograph of the unstrained model the thickness contour fringes may be numbered consecutively from the arbitrarily numbered starting point along any line, straight or curved. On the photograph of the strained model the fringes are again numbered consecutively along the arbitrary line or curve from the same arbitrarily numbered starting point. If plots of these arbitrary fringe numbers along the line or curve are made, graphical subtraction will yield the fringe shift or relative fringe order along the line.

Another scheme for obtaining the isopachic fringe order is to utilize the moire effect.

The moire effect is an optical phenomenon observed when two arrays of lines are superimposed. If the arrays consist of opaque

lines which are not identical in spacing or orientation, then moire fringes will form as lines of one array alternately fall on or between the lines of the other array. This phenomenon can be observed by placing two pieces of ordinary screen wire together.

To aid in visualizing the moire effect consider the array of lines shown in Fig. 6.

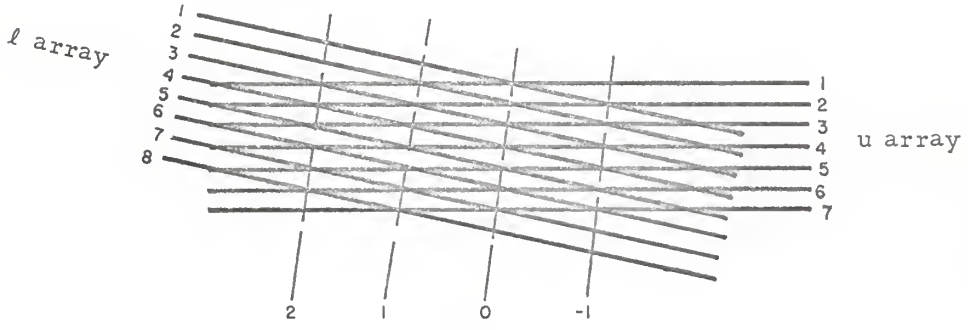

Fig. 6. Moire fringes.

It will be noticed that if the intersection of the "u" array and the "ℓ" array are connected as shown, the lines so formed are the loci of constant line number difference. Along these loci alternately dark and light patterns are observed. Between the lines of constant line number difference the "u" and "ℓ" array lines approach each other more closely and form areas of gray or black.

If the lines of the "u" array are considered to be the thickness contour fringes exhibited by the unloaded model and the lines of the "ℓ" array those exhibited by the loaded model it is evident that, if superimposed, the load and no load fringe patterns will produce a moire

effect giving lines of constant fringe number difference. In other words, the moire pattern produced will give the loci of points along which the thickness fringe shift between load and no-load conditions is constant and hence the isopachic pattern.

The procedure then is to print through the properly superimposed negatives of the strained and unstrained model. An alternate procedure is to double expose one film with the load and no-load thickness contour fringe patterns.

EXPERIMENTAL CONSIDERATIONS

The foregoing has implied restrictions that require further discussion.

Since distinct thickness interference fringes require a unique velocity of light through the model, the model material must not be permanently or artificially birefringent. Photoelastic materials, on the other hand, should be highly birefringent. Acrylic plastics such as plexiglass exhibit very small artificial birefringence and were found to be satisfactory. Glass falls into the same category. The material fringe values of plexiglass and glass are 500 and 800, respectively (4). These figures are lower limits and may be compared with a material fringe value of 100 for a common photoelastic material such as CR 39. The plexiglass used was found to have a material fringe value of 800.

In plexiglass, stresses may be used in the elastic range up to about 1500 lb/in.^{2}. This corresponds to an isopachic fringe order of about 20. This is comparable to the number of isochromatic fringes that can be obtained. Of course the number that can actually be observed depends upon the initial thickness contour fringe pattern and geometrical distortion in plane of model.

Using materials whose surfaces have been made partially reflecting the transmitted light in Fig. 4 will produce interference patterns. Interference patterns may be observed with untreated materials only from the reflected light. The transmission method has the advantage that the direction of the light observed is not seriously affected by tipping or warping of the model under load whereas the reflected rays are.

In models of appreciable thickness the light source must be highly monochromatic. Referring to Fig. 7 it is seen that, if λ in the basic formula $N\lambda = 2\mu t$ takes on a small range of values, the fringes will appear as bands instead of distinct lines. If a conservative criterion for distinct fringes is set as a maximum permissible broadening of 1/4 of the distance between fringes, the maximum width of the spectral band $\Delta\lambda$ is $\Delta\lambda = \frac{\lambda}{4N}$.

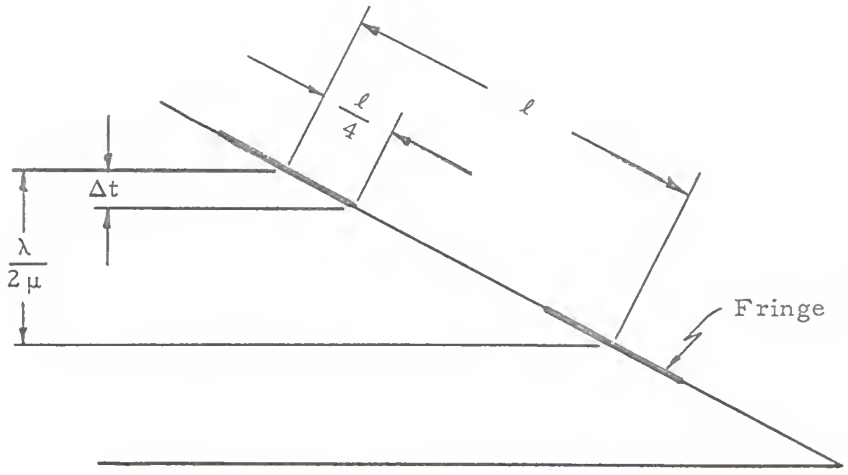

Fig. 7. Fringe broadening.

For most practical photoelastic analyses, model thicknesses range from 1/16 in. to 1/2 in., giving rise to interference fringe orders between 7,500 and 60,000 from $N\lambda = 2\mu t$ with λ in the green region ($5460A^{o}$) and $\mu = 1.5$. For a model 1/4-in. thick, the nominal fringe order is 30,000 permitting a spectral band width of only 0.05 angstrom units. This is very near the limiting minimum effective band width for ordinary low-pressure mercury vapor lamps (2). The use of thicker models is possible, but the fringes become indistinct.

A sodium vapor lamp may be employed if a little trick is used (9). Since sodium light contains a line doublet ($5890A^{o}$ and $5896A^{o}$) the sets of interference fringes produced by the doublet may overlap

and disturb the moire effect if the model thickness is not just right. Since the variation in thickness is a small fraction of the nominal model thickness only a few hundred fringes at the most will appear in the fringe patterns. If the model thickness is correct, the fringe order at a point associated with one line of the doublet may be a small integer different from the fringe order associated with the other lines. Then for a few hundred fringes the overlapping will be of no serious consequence. Thus the trick is to tilt the model very slightly away from normal incidence until the clearest system of fringes appears.

If photographs of the fringe pattern are to be made, the intensity of the light source should be great enough to make the exposure time reasonable.

The initial uniformity of the model material must be such that it does not display excessively high fringe densities. In regions of high stress gradient the thickness changes produced by loading would be expected to cause the fringes to become densely spaced, and they would become impossible to distinguish. By careful selection of model materials, so that in areas of supposed high stress concentrations the initial fringe density is small, this difficulty can be overcome. Of course, if the stress gradient is large enough the elastic limit of the material will be exceeded and the method fails anyway, in that the equations of elasticity no longer apply.

The requirement of small initial fringe densities will be met if the model is wedge-shaped at least in the area of interest. Commercial acrylic plastics should be suitable in that they are cast between

plate glass. By pretest, areas displaying a desirable initial fringe distribution can be found. It must be pointed out that only the thinner sheets of such material (1/16 in. to 1/4 in.) will display small enough thickness variations to be useful.

The loading of the model should be such that the plane stress condition is produced exactly; i.e., the loading must not vary throughout the thickness of the plate model.

The optical geometry must provide a wide stream of uniformly distributed light perpendicular to the plane of the model. This may be accomplished by using long distances between the light source and the model. Mesmer (6) has suggested the arrangement shown in Fig. 8, using a partially reflecting mirror and a lenses.

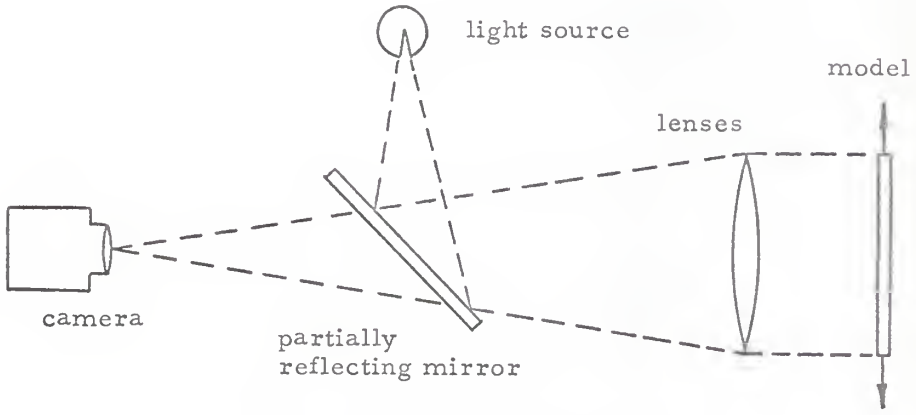

Fig. 8. Simple interferometer.

Care must be exercised in cutting the model. If excessive heat is developed along cuts, residual stresses will be developed which cause such extreme thickness variations that no interference fringes at all may be observed along the edges of the model.

From Fig. 6 it may be observed that the moire lines or lines of constant line number difference are approximately perpendicular to the "unloaded" or initial fringes. Therefore if the moire technique is to be used, the model should be cut so that the initial interference fringes are approximately perpendicular to the known or guessed isopachic pattern.

If the isopachic pattern is to be produced by printing through the superimposed negatives of the fringe pattern in the loaded and unloaded condition, the coincidence of the negatives must be exact. This could be accomplished by marking the model so that exact alignment would be possible. Some sort of device incorporating micrometer screws for moving the negatives relative to one another would facilitate this operation. If the deformations are small, one film can be double exposed with the load and no-load fringe patterns.

Film, developers, and printing paper used must be such as to produce maximum contrast with a minimum of graininess.

EXPERIMENTAL SETUP AND PROCEDURE

In that no facilities were available for producing partially reflecting surfaces on the model material, the reflection technique was used.

To obtain the isopachic pattern directly, the moire effect was utilized with the isopachic pattern being obtained by double exposure of the loaded and unloaded model on the same film. Initial attempts were made to print through the separate negatives by superimposing them by

hand but exact coincidence was almost impossible to obtain. The double exposure technique proved to be entirely satisfactory. Of course the relative fringe order could be plotted for the load and no-load state, and graphical subtraction of the plots would yield the isopachic fringe order.

The optical arrangement shown in Fig. 8 is undoubtedly one of the best possible but in that no large lenses or half silvered mirror were available, and the cost of purchasing them was prohibitive, an alternate optical arrangement was dictated. It was decided to utilize the optical elements of the polariscope of the K. S. U. Experimental Stress Analysis Laboratory to the greatest extent possible. The arrangement used is as shown in Fig. 9 and Plate I.

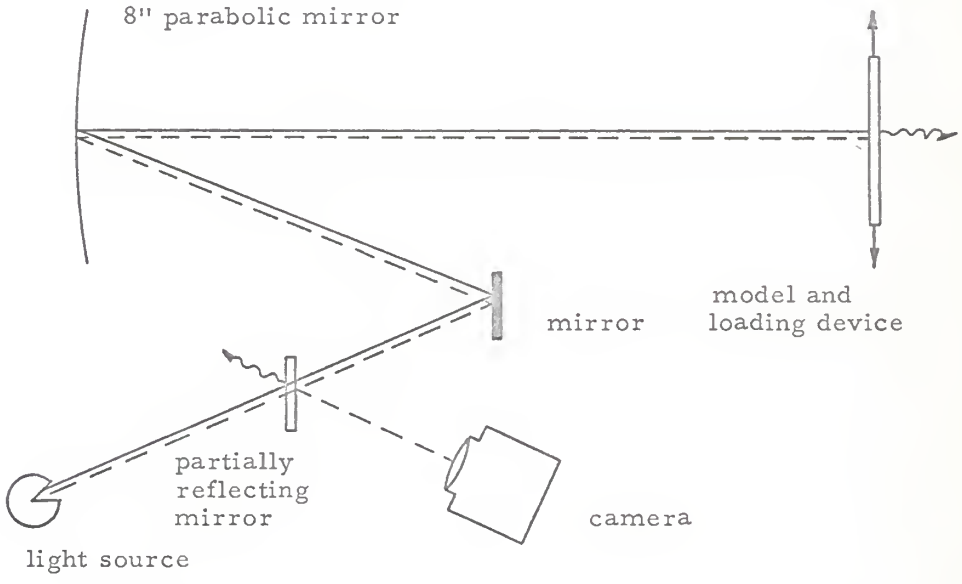

Fig. 9. Experimental arrangement.

EXPLANATION OF PLATE I

(1) mirror
(2) partially reflecting mirror
(3) light source
(4) eight-inch parabolic mirror

PLATE I

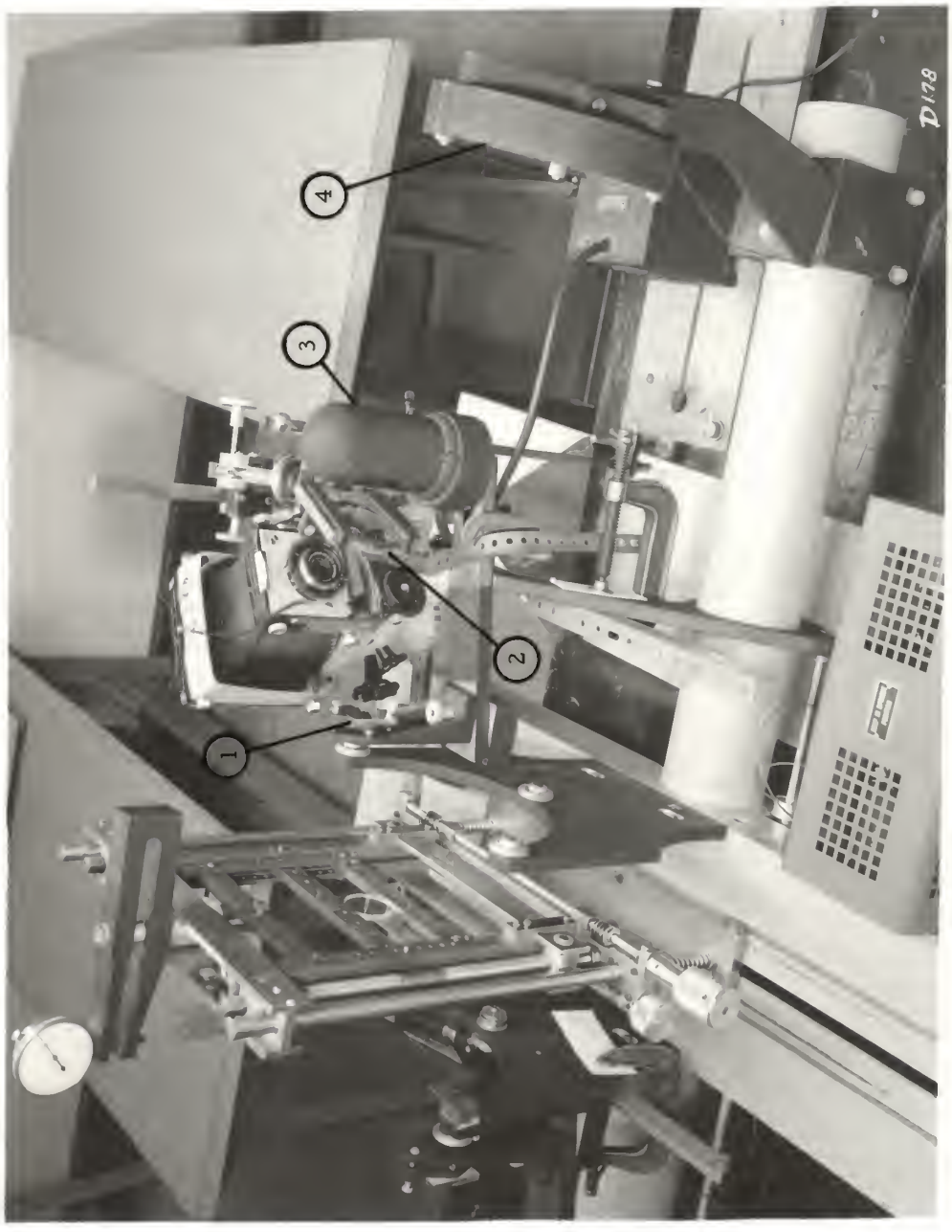

The utilization of the polariscope proved to be particularly advantageous in that it is equipped with an integral loading frame so no construction was necessary along this line. The small partially reflecting mirror (reflectance 33 per cent) was the only optical component purchased. An adjustable frame was constructed to hold it and the camera was mounted by means of angle irons clamped to the frame of the polariscope.

The light rays originating at the source travel to the partially reflecting mirror which passes a portion of them and reflects the remainder. The latter portion is in effect wasted. The transmitted portion travels to the model by way of the small mirror and the parabolic mirror both of which are integral to the polariscope. At the model two-beam interference takes place and the reflected rays travel back to the partially silvered mirror along the same path. At this point they are again reflected and transmitted with the former portion becoming available for photography. Denoting the intensity of the light source by I, the reflectance of the partially silvered mirror by p and that of the model by q, the light reaching the camera is given by $(1 - p)(pq - I)$. Taking the reflectance of the model as 4 per cent and that of the mirror as 33 per cent, the light intensity available for photographic purposes is $9.64\,(10^{-4})$ that of the source. Hence an intense light source was necessary to avoid excessively long exposure times.

A mercury vapor lamp was tried initially but was not satisfactory in that the light was not sufficiently monochromatic. Fringes appeared upon firing but disappeared almost immediately due to pressure broadening (2). A sodium vapor lamp was substituted and found by trial to be sufficiently monochromatic. It was used as the light source.

The model material used was the acrylic plastic methyl methacyrlate, which is manufactured under the trade name plexiglass. One quarter inch, 1/8 in., and 1/16 in. sheets of the type II, clear, ultraviolet absorbing material with polished faces were obtained.

The selection of the region from which the model was to be cut was accomplished by pretest. Each sheet of plexiglass was placed in the optical train at the loading frame and visual observation made at the camera location to determine whether the material displayed suitable initial thickness interference fringes. The 1/4-inch sheet displayed a perfect Newton's ring in a region too small to be used as a model, and no fringes in any other location. The 1/8-inch sheet, however, displayed fringes over its entire area with the fringes varying smoothly in density and width from point to point hence affording a wide selection of regions from which a model could be cut.

A Linhof 4 by 5 Color Camera was mounted as shown in Fig. 9 and Plate I at the focal point of the optical train. A Goertz "Red Dot" Artar lense with a focal length of 8-1/4 inch was used. This arrangement produced a negative which was 0.265 times as large as the model. The maximum f number available was 9, and the exposure times possible ranged upward from 1/400 sec. as desired. The camera was

equipped with a ground glass back so that visual observation of the image could be made before the film was inserted.

Kodak Contrast Process Panchromatic film was used. This is a fine grain, panchromatic, antihalation film of very high contrast (5). It gives sharp separation of light and dark tones, and is sensitive from approximately 3600A° to 6500A°. The correct exposure is critical if maximum contrast is desired. For single exposures an f number of 16 and a shutter speed of 1/5 sec. were used. For double exposures, the f number and shutter speed were 22 and 1/5 sec., respectively.[1] Kodak D-11 developer was used for processing the film as recommended (5).

Because of the small negatives produced, enlargement was necessary during the printing process. The negatives were enlarged approximately 8 times on Kodabromide F-4 single weight printing paper. The f number on the enlarger lense was 5.6, and the exposure times were 15 sec. and 30 sec. for single exposed and double exposed negatives, respectively.

The integral loading frame was modified by tapping holes in its base to receive adjusting screws so that it could be tipped off vertical. By doing this the model could be moved slightly relative to the impingent light rays.

---

[1] The light source varied in intensity from day to day, so no optimum exposure was found. The figures given represent the best results obtained.

The model was placed in the loading frame and a slight load applied to hold it in place. It was then adjusted relative to the light field until the clearest image was observed through the ground glass camera back.[2] The model was then unloaded, and five minutes allowed for it to return to its unstrained state. This was done to compensate for any creep that might have been present. The desired exposures of the unloaded model were then taken. The model was then loaded slowly to the desired point and the desired exposures made immediately. Extreme care was exercised in placing the model in the loading frame in an effort to ensure that the state of plane stress was obtained.

The models were cut to the desired shape using a high speed milling machine. Care was exercised in order to minimize the stresses produced by this operation.

VERIFICATION

The isopachic calibration constant $K = \lambda E/2 \mu \nu$ was determined experimentally using a beam loaded in pure bending as shown in Fig. 10.

---

[2] Models with very fine initial patterns produced the moire effect with the ground glass of the camera back, and adjustment was made difficult for such models.

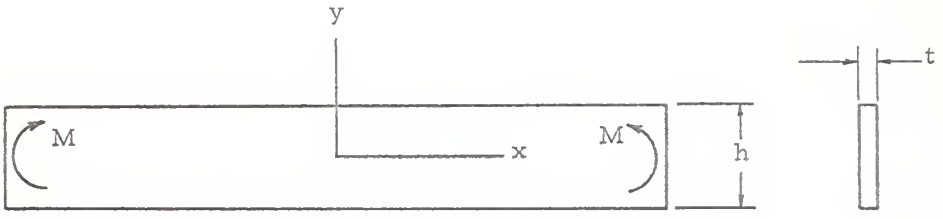

h = 0.971 in.
t = 0.114 in.

Fig. 10. Calibration beam.

From the familiar relation $\sigma_{1\ max} = \frac{6M}{th^2}$, it is seen that $\frac{6M}{th^2} = \frac{K}{t}\Delta N$. Hence,

$$K = \frac{6M}{\Delta N h^2} \tag{23}$$

Using 1500 lb/in.^{2} as the elastic limit for plexiglass, it was found that maximum moment that could be applied was 26.8 in.-lb.

Plate II shows the middle section of the beam in the unstrained and strained states. Plate III shows the isopachic patterns obtained by double exposure.

The isopachic fringe order of the beams of Plate III was obtained directly. As a check, the fringe order was obtained from the figures of Plate II by graphical subtraction as shown in Fig. 15.

EXPLANATION OF PLATE II

Fig. 11. Thickness contour fringes of the unstrained calibration beam.

7.5 fringes/in.

Fig. 12. Thickness contour fringes of the strained calibration beam.

M = 15.64 in.-lb.

PLATE II

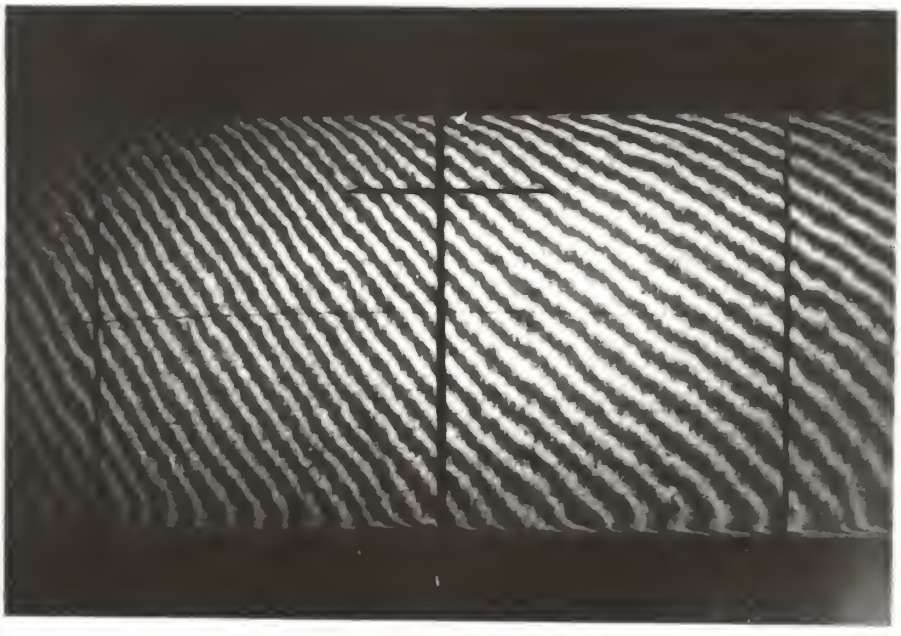

Fig. 11

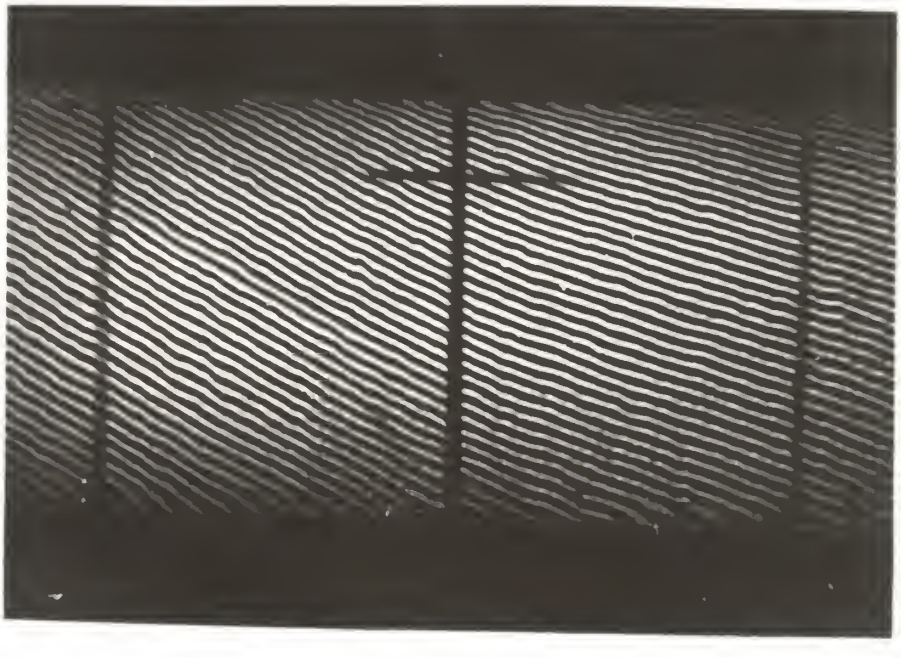

Fig. 12

EXPLANATION OF PLATE III

Fig. 13. Isopachic pattern of calibration beam.
$M = 7.53$ in.-lb.
$\Delta N = 4.9$

Fig. 14. Isopachic pattern of calibration beam.
$M = 15.64$ in.-lb.
$\Delta N = 10.1$

PLATE III

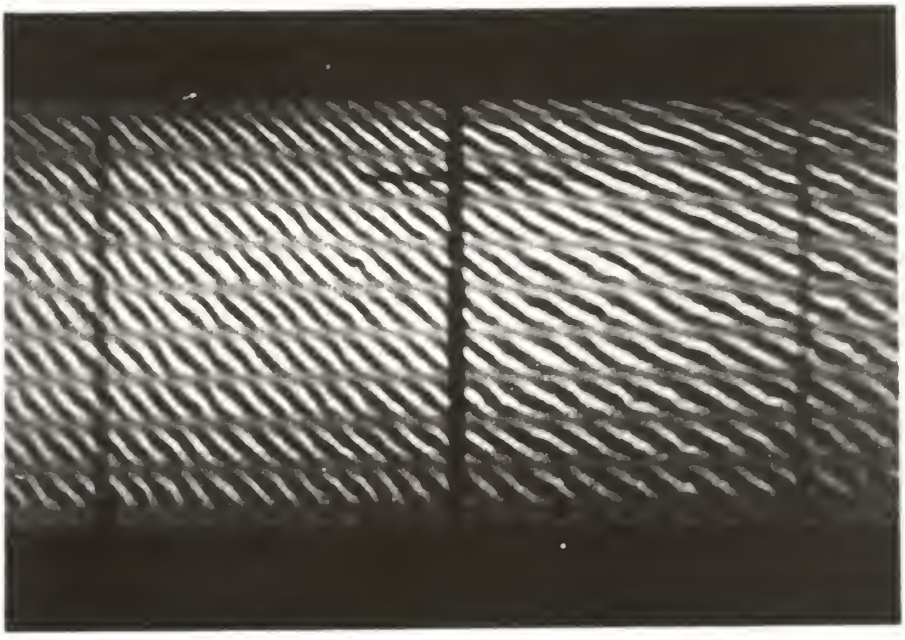

Fig. 13

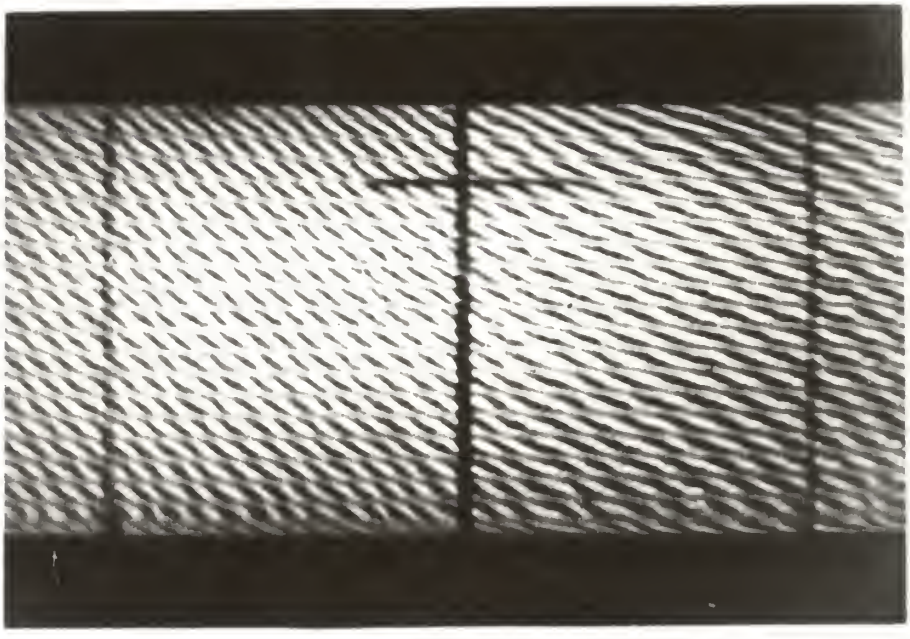

Fig. 14

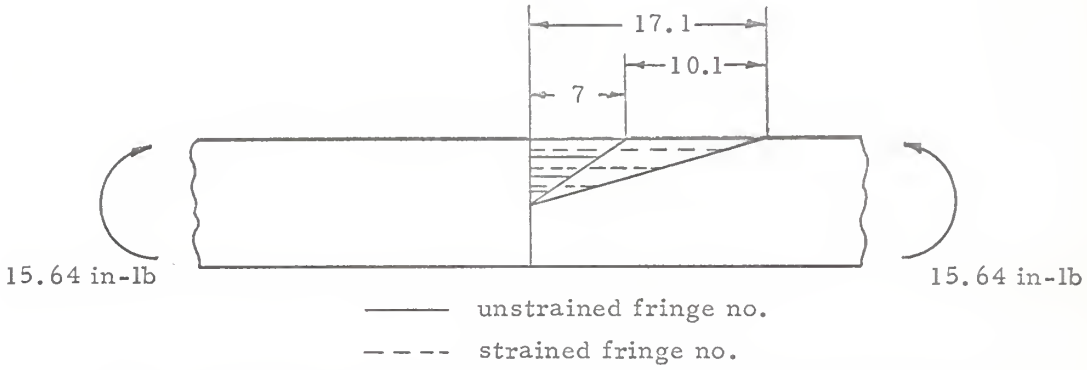

Fig. 15. Graphical determination of the isopachic fringe order.

The isopachic calibration constant was found to be

9.855 lb/in.fringe by Eq. (23).

The diametrically loaded disk was chosen as the model shape to be used to compare the theoretical and experimental analyses.

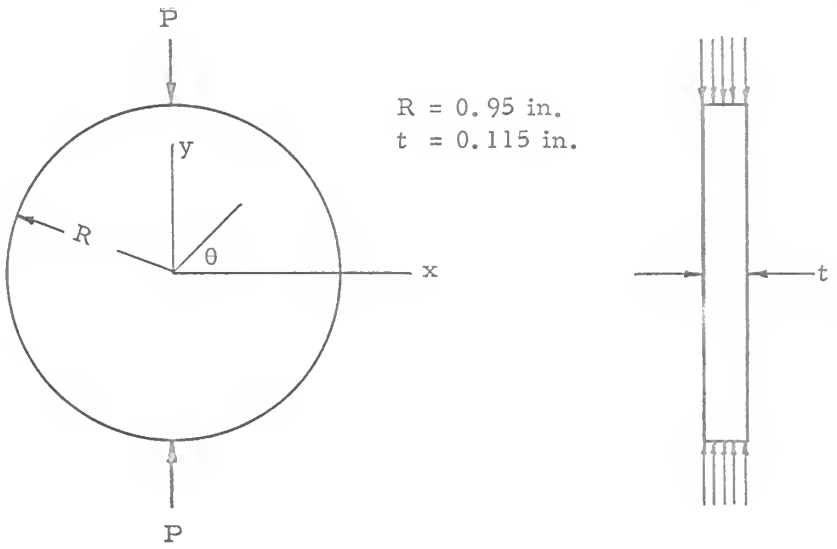

Fig. 16. Model shape.

The theoretical stress distribution (3, 10) in Cartesian co-ordinates throug the center of the disk is given by

$$\sigma_1 = \frac{P}{Rt} - \frac{4PR}{t}\left[\frac{x^2}{(x^2+y^2+R^2)^2 - 4R^2y^2}\right] \tag{24a}$$

and

$$\sigma_2 = \frac{P}{Rt} - \frac{4PR}{t}\left[\frac{R^2-y^2}{(x^2+y^2+R^2)^2 - 4R^2y^2}\right]. \tag{24b}$$

Adding:

$$\Sigma = \frac{2P}{Rt}\left[\frac{(x^2+y^2+R^2)^2 - 2R^2(x^2+y^2+R^2)}{(x^2+y^2+R^2)^2 - 4R^2y^2}\right] = \frac{-K}{t}\Delta N. \tag{25}$$

The theoretical result in polar co-ordinates is given by

$$\Sigma = \frac{2P}{Rt}\left[\frac{r^4 - R^4}{(r^2+R^2)^2 - 4r^2R^2\sin^2\theta}\right] = \frac{-K}{t}\Delta N. \tag{26}$$

Solving for r with $A = \frac{2P}{\pi RK}$:

$$r^2 = R^2\left[\frac{-\Delta N\cos 2\theta \pm \sqrt{\Delta N^2\cos^2 2\theta + (\Delta N + A)(A - \Delta N)}}{\Delta N + A}\right] \tag{27}$$

This relation was used to compute the theoretical isopachic fringe values of Plate XI.

The sum of the principal stresses along the x axis is given by

$$\Sigma_{x,o} = \frac{2P}{\pi Rt}\left[\frac{x^2 - R^2}{x^2 + R^2}\right] = -\frac{K}{t}\Delta N. \tag{28}$$

Hence along the x axis:

$$x^2 = R^2\left[\frac{A - \Delta N}{A + \Delta N}\right]. \tag{29}$$

This solution was used to calculate the theoretical isopachic fringe values of Plate XII.

The sum of the principal stresses along the y axis is given by

$$\Sigma_{o,y} = \frac{2P}{\pi Rt}\left[\frac{y^2 + R^2}{y^2 - R^2}\right] = -\frac{K}{t}\ \Delta N. \tag{30}$$

Hence along the x axis:

$$y^2 = R^2\left[\frac{\Delta N - A}{\Delta N + A}\right] \tag{31}$$

The theoretical values of Plate XIII were obtained from this relation.

It will be noted that the theoretical fringe value at the center of the disk is given by

$$A = \frac{2P}{\pi RK} \tag{32}$$

while the fringe order along the circumference of the disk is zero.

Three models were used to determine the best initial fringe pattern for distinct isopachic patterns. The models displayed fringe densities of 12, 24, and 40 fringes/in. with fringe widths of 0.05, 0.0125, and 0.01 inch, and will be called the coarse, medium and fine screen models, respectively.

Plates IV through IX show these disks loaded with the initial fringe pattern perpendicular to the load, while Plate X shows the isopachic pattern with the load parallel to the initial fringe pattern.

Two loads were used for each model. They were 44.24 lb and 88.48 lb which gave theoretical isopachic fringe orders of 3.01 and 6.02, respectively, at the center of the disk. The elastic limit with these loads was theoretically reached on the y axis at y = 8.48R

EXPLANATION OF PLATE IV

Fig. 17. Coarse screen initial interference pattern immediately after model was cut.

Fig. 18. Coarse screen initial interference pattern two months after the picture of Fig. 17 was taken.

PLATE IV

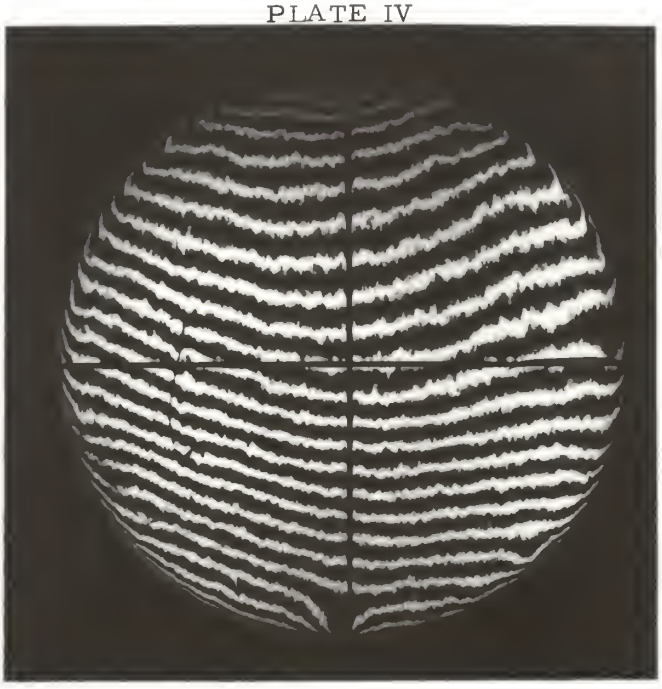

Fig. 17

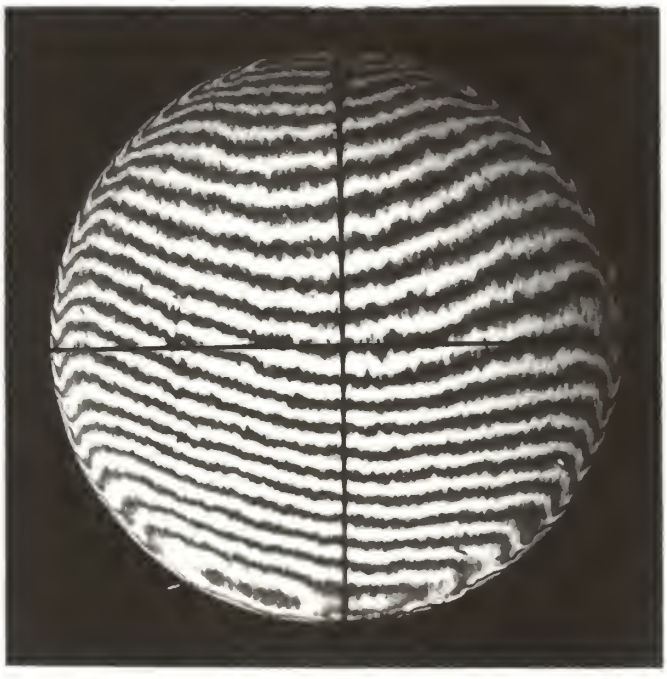

Fig. 18

EXPLANATION OF PLATE V

Fig. 19. Coarse screen interference fringes.
P = 88.48 lb.

Fig. 20. Coarse screen isopachic pattern.
P = 88.48 lb.

PLATE V

Fig. 19

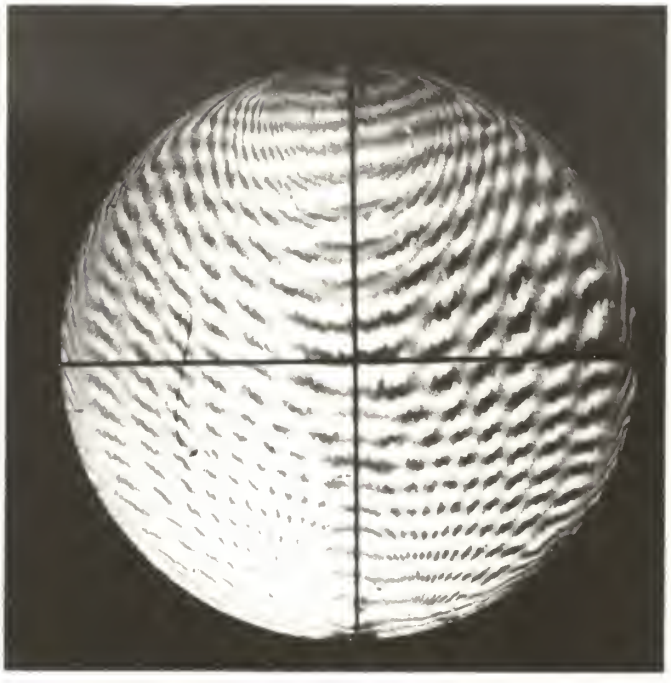

Fig. 20

EXPLANATION OF PLATE VI

Fig. 21. Medium screen initial interference fringes.

Fig. 22. Medium screen interference fringes.
P = 44.24 lb.

PLATE VI

Fig. 21

Fig. 22

EXPLANATION OF PLATE VII

Fig. 23. Medium screen isopachic pattern.
P = 44.24 lb.

Fig. 24. Medium screen isopachic pattern.
P = 88.48 lb.

PLATE VII

Fig. 23

Fig. 24

EXPLANATION OF PLATE VIII

Fig. 25. Fine screen initial interference pattern.

Fig. 26. Fine screen interference pattern.
P = 44.24 lb.

PLATE VIII

Fig. 25

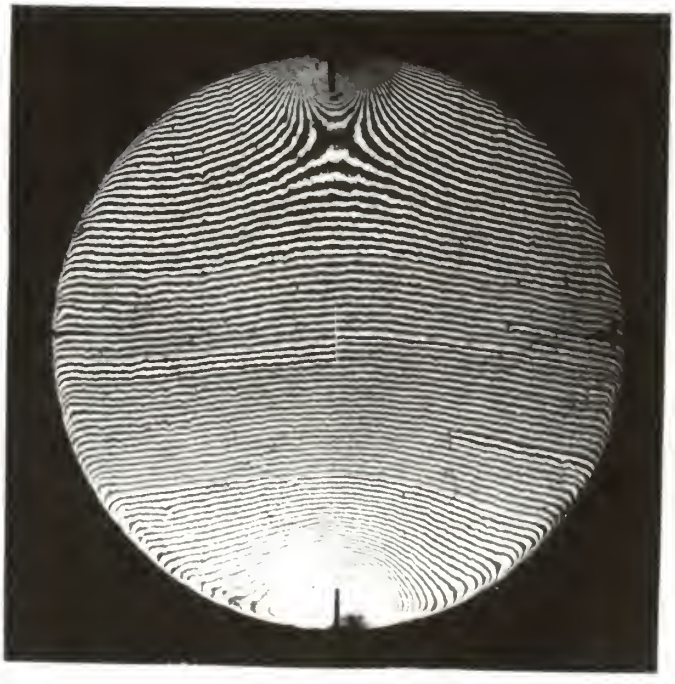

Fig. 26

EXPLANATION OF PLATE IX

Fig. 27. Fine screen isopachic pattern.
P = 44.24 lb.

Fig. 28. Fine screen isopachic pattern.
P = 88.48 lb.

PLATE IX

Fig. 27

Fig. 28

EXPLANATION OF PLATE X

Fig. 29. Coarse screen interference pattern with the initial pattern parallel to the load.
P = 44.24 lb.

Fig. 30. Coarse screen isopachic pattern with the initial pattern parallel to the load.
P = 44.24 lb.

PLATE X

Fig. 29

Fig. 30

EXPLANATION OF PLATE XI

Theoretical and experimental isopachic fringes.

PLATE XI

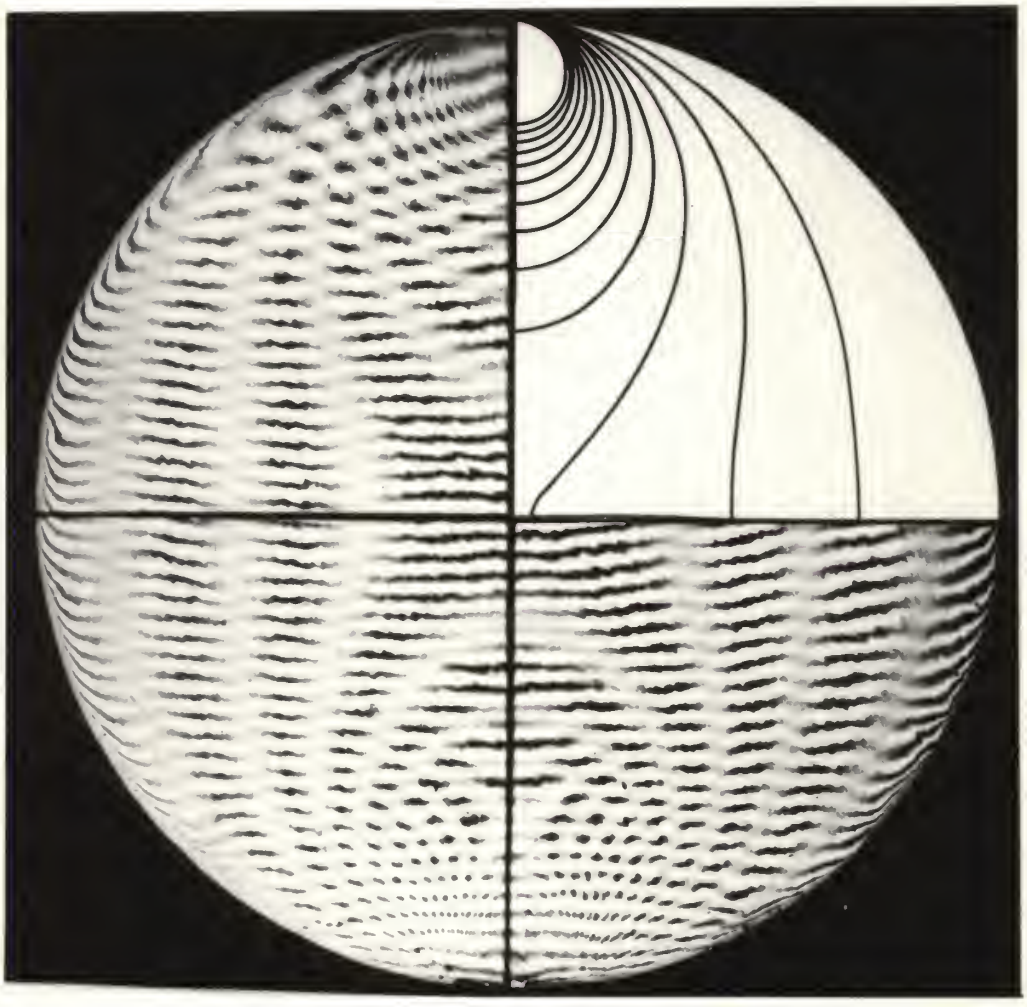

EXPLANATION OF PLATE XII

Isopachic fringe order along the horizontal axis.
P = 88.48 lb.

PLATE XII

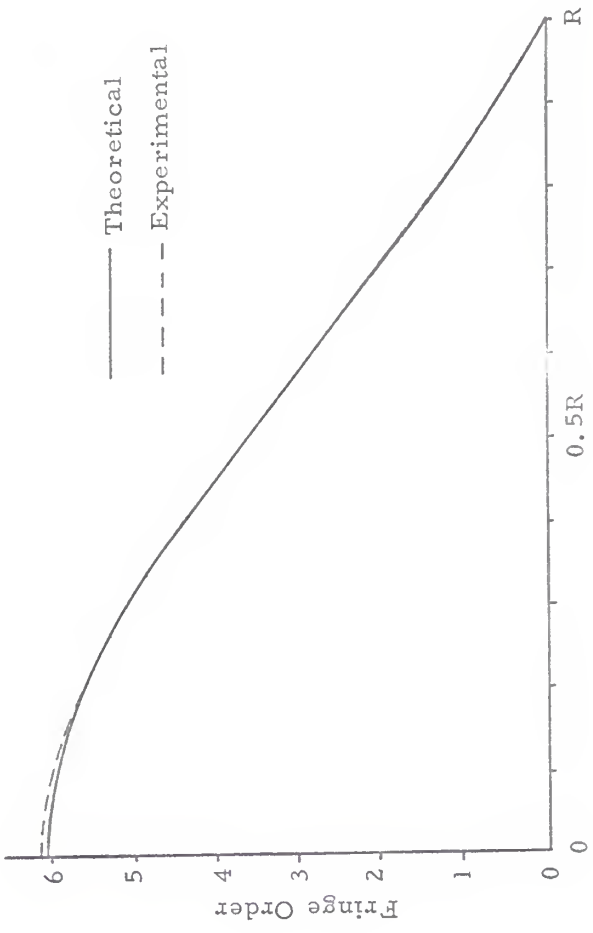

EXPLANATION OF PLATE XIII

Isopachic fringe order along the vertical axis.
P = 44.24 lb.

PLATE XIII

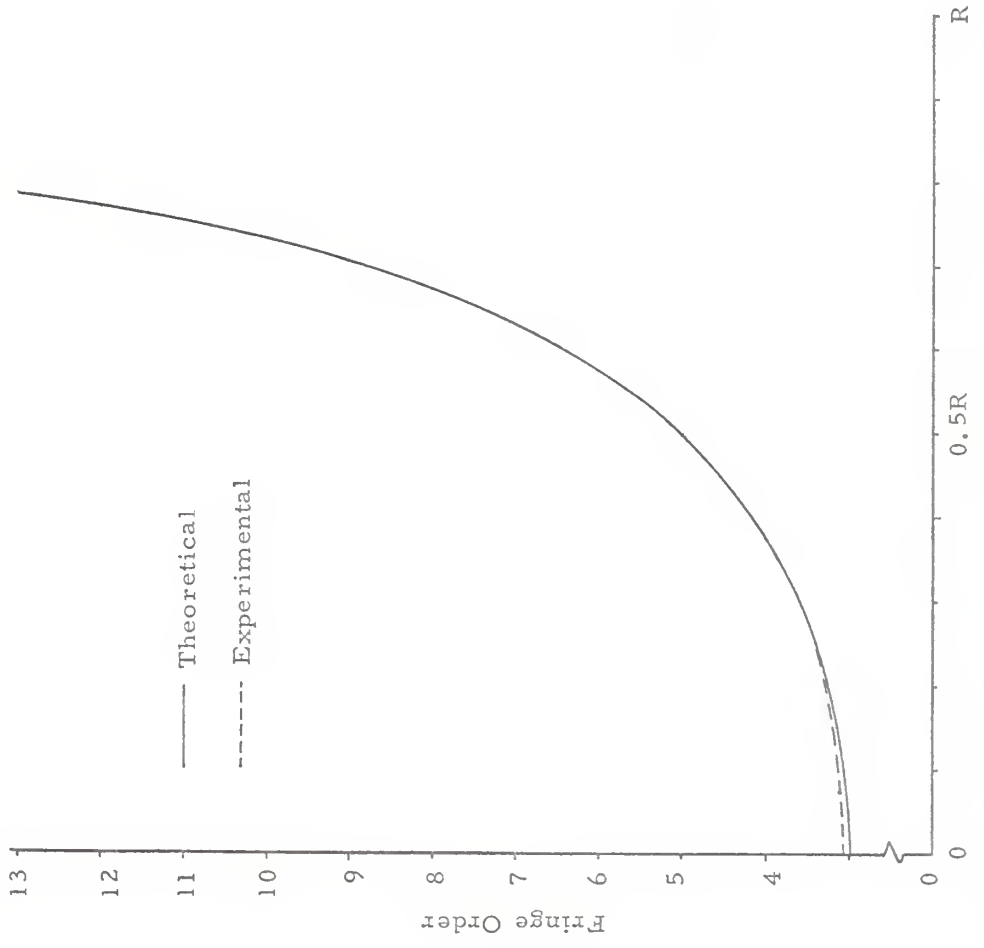
Fringe Order
13
12
11
10
9
8
7
6
5
4
0
0
0.5R
R
Theoretical
Experimental

and $y = 6.97R$, respectively. These figures correspond to a theoretical maximum obtainable isopachic fringe order of

$$\frac{1500}{9.855\,(0.115)} = 17.4 \text{ lb/in. fringe}$$

at the elastic limit.

Plates XI, XII and XIII show both theoretical and experimental results.

CONCLUSIONS AND RECOMMENDATIONS

From Plates XI, XII and XIII it is seen that the experimental results agree very well with those expected from theoretical considerations. The slight discrepancy noted at the center of the disk in Plates XII and XII is due in part to difficulty in determining the exact fringe order there. In the opinion of the author, the agreement between experimental and theoretical solutions fully corroborates the validity of the experimental method.

Plate XIII shows the experimental and theoretical results only up to an isopachic fringe order of 13 at $y = 0.79R$ on the vertical axis. This was with the model loaded to 44.24 lb. Higher order fringes became difficult if not impossible to distinguish. Of course it would be unreasonable to compare analyses in the vicinity of $y = R$, since the loading conditions are not the same for the experimental and theoretical problems.

The difficulty in distinguishing the higher order isopachic fringes was to be expected. In regions of high stress the interference fringes

were very closely spaced as Figs. 19, 22, 26 and 29 show clearly in the vicinity of $y = R$. The initial interference fringes on the other hand were not so dense there. Hence upon superposition of the two systems of fringes the loaded set was obliterated, and all that could be seen was the initial pattern as Figs. 20, 23, 24, 27, 28, 29 and 30 indicate.

A comparison of Figs. 23, 24, 27 and 28 indicates that the obliteration effect became worse with the finer initial patterns. Thus the coarse screen model should have produced the best isopachic patterns near $y = R$. Examination of Fig. 18 shows that this was not the case, however. Even though the initial pattern was not dense, the fringe widths were so large as to produce the obliteration effect with any other set of fringes when superimposed. The ideal model, of course, would display no initial fringes near the load so that the loaded pattern would be the isopachic pattern. Post (8) has devised a photoelastic interferometer that eliminates this difficulty. The highest fringe number that could be distinguished at the higher loading was 15 at $y = 0.65R$.

Along the horizontal axis with correspondingly lower stresses the fine screen model would have been expected to produce better isopachic patterns. No significant difference in the isopachic fringes produced by the different models could be detected by the author, however. It can then be concluded that the best isopachic patterns were obtained from the medium screen model with a fringe density of 24 fringes per inch and a fringe width of 0.0125 in. This was as expected from preliminary considerations.

The pictures shown in Figs. 17, 21 and 25 were taken immediately after the model was cut. The stresses produced by the cutting operation are evident in the curved initial fringes near the boundary of the disk. The picture shown in Fig. 18 was taken two months after that of Fig. 17. Both figures show the same model; the only difference being the time lapse. As an interesting sidelight notice the change in the initial fringe pattern near the boundary due to thickness changes arising from humidity and temperature variation.

Figures 29 and 30 show the coarse screen model loaded with its initial fringes parallel to the load. This was done in order to determine whether the initial fringe pattern should indeed be approximately perpendicular to the known or supposed resulting isopachic pattern. It should, as the figures obviously indicate, in that the isopachic set in this case are not as distinct as those in which the initial pattern is perpendicular to the isopachic pattern.

The experimental results shown are the result of many trials, some more successful than others. The greatest difficulty with the experimental procedure was obtaining a true two-dimensional stress state. Initial attempts at matching experimental and theoretical analyses met with no success. The experimental results were off as much as one fringe at the lower loading which represented an error of 33 per cent. The higher loading produced results which were a maximum of 14 per cent in error. This reduction in error with larger loading indicated that the loading device was at fault after the calibration constant was checked and found to be correct. Adjustment of the loading frame to eliminate as much friction as possible and extreme care in placing the

model in the loading frame produced the isopachic patterns shown. With the equipment available, this is the chief drawback of the experimental method.

The negatives produced by the optical train were too small to be directly useful. The enlargement necessitated by their small size was a definite drawback. Had the negatives been large enough to examine directly, much time could have been saved in arriving at a suitable experimental procedure and evaluation of results.

The technique of double exposing the film with the initial and loaded interference fringes proved to be quite satisfactory with the model shape used. For the more general case displacements in the plane of the model may become large enough to necessitate superimposures of separate negatives in the area of interest.

The film used proved to be entirely satisfactory. It is felt by the author that it would have been even more so if the exact exposure necessary could have been found. The printing paper and development technique were adequate. Added contrast would have been an improvement, however.

The following recommendations are made by the author: First, the procedure discussed here would be greatly improved if a more refined loading device were constructed. This device should enable the true two-dimensional state of stress to be achieved. Also, it should be constructed so that it could be moved relative to the light field around the horizontal and vertical axes. This would facilitate the alignment of the model relative to the light field. Second, a camera

with a longer focal length should be used so that larger negatives could be obtained. A device for superimposing the strained and unstrained exposures should be constructed if more general stress states are to be investigated. Last, it is recommended that Kodabromide F-5 instead of F-4 paper be used for printing, and that D-8 developer in place of D-11 be used for developing the exposed film (5).

The isopachic method described here may be used when initial stresses are present, in that the superposition yields the effects due to loading only. It may theoretically be used to determine stresses due to dynamic loadings whereas the classical separation techniques may not, since they require the assumption that the body forces in the equations of equilibrium are negligible or zero. The technique may also be used in plastic range to measure displacements. By printing or ruling a fine system of lines on a model, displacements in the plane of the model may be determined through the moire effect (7, 11, 12, 13).

The isopachic method described here is the best, in the author's opinion, of the isopachic methods presently available. All of the other practical systems are tedious point by point methods, or else require highly elaborate equipment and intricate techniques.

ACKNOWLEDGMENT

The author wishes to express his thanks to Professor F. J. McCormick for his supervision and guidance in writing this report.

REFERENCES

1. Coker, E. G. and L. N. G. Filon. Photoelasticity. New York: Cambridge, 1957. 720p.

2. Curry, C. Wave Optics. London: Edward Arnold, 1957. 155p.

3. Frocht, M. M. Photoelasticity. Two volumes. New York: John Wiley and Sons, 1948.

4. Jessop, H. T. and F. C. Harris. Photoelasticity. New York: Dover Publications, 1960. First published by Cleaver-Hume Press, 1949.

5. Kodak Reference Handbook, "Black and White Processing and Printing." New York: Eastman Kodak.

6. Mesmer, G. "The Interference Screen Method." Proc. S.E.S.A., 1956, 13 (2) : 21.

7. Morse, S., A. J. Durelli and C. A. Sciammaralla. "Geometry of Moire Fringes in Strain Analysis." Journal of the Engineering Mechanics, August 1960, 86 (EM 4): 105-126.

8. Post, D. "A New Photoelastic Interferometer Suitable for Static and Dynamic Measurements." Proc. S.E.S.A., 1954, 12 (1): 191.

9. Post, D. "Photoelastic Stress Analysis for an Edge Crack in a Tensile Field." Proc. S.E.S.A., 1954, 12 (1): 99.

10. Post, D. "Photoelastic Evaluation of Individual Principal Stresses." Proc. S.E.S.A., 1956, 13 (2): 119.

11. Riley, W. F. and A. J. Durelli. "Application of Moire Methods to the Determination of Transient Stress and Strain Distributions." Journal of the Applied Mechanics, 29 (E-1): 23-39.

12. Sciammarella, C. A. and A. J. Durelli. "Geometry of Moire Fringes in Strain Analysis." Journal of the Engineering Mechanics, August 1960, 86 (EM 4): 105-126.

13. Ibid. "Moire Fringes as a Means of Analysing Strains." Feb. 1961, 87 (EM 1): 55-74.

A NEW METHOD FOR OBTAINING ISOPACHIC PATTERNS

by

JAMES REVELL KIMZEY

B. S., M. E., University of Arkansas, 1961

AN ABSTRACT OF A MASTER'S REPORT

submitted in partial fulfillment of the

requirements for the degree

MASTER OF SCIENCE

Department of Applied Mechanics

KANSAS STATE UNIVERSITY
Manhattan, Kansas

1963

Effective methods of obtaining isopachic patterns in plane stress structures and models have been sought for the last half century. The isopachic pattern describes the thickness changes caused by loading a two-dimensional model and therefore represents the sum of the principal stresses at all points of a plane stress system. When used in conjunction with the conventional isochromatic pattern of photoelasticity, which represents the difference of the principal stresses at all points in a model, simple evaluation or separation of the individual principal stresses is made possible.

A brief review of the theory of photoelasticity is presented. The equations from the theory of elasticity that are necessary to utilize the photoelastic technique are set forth along with the conventional methods for obtaining the individual principal stresses. The conventional methods reviewed are: integration of the equations of equilibrium, numerical solution of Laplace's equation, and the existing methods for obtaining isopachic patterns. In the latter section simple two-beam interference is discussed and the manner in which it may be utilized to obtain directly the isopachic pattern for optically flat models is pointed out.

The new isopachic method does not require an optically flat model. The model must be essentially wedge shaped at least in the area of interest. Hence thickness contour interference fringes are observed initially. These fringes move to new locations under the action of applied stresses. The number that move past a given point is pro-

portional to the thickness change produced and hence to the sum of the principal stresses.

Three methods for analyzing the thickness contour interference fringes produced by the new method are discussed briefly. The chief among these makes use of the moire effect.

From the theory of the new method the experimental technique must meet several criteria. These are discussed, and the setup and procedure actually used to verify the method are given.

The diametrically loaded disk was chosen as the model shape to be used to compare the analyses of the new method with the theoretical analyses available from the theory of elasticity. Three disks were used with different initial thickness contour interference fringe patterns. The experimental results are given and compared with the theoretical results.

Several recommendations are made by the author which would improve the experimental techniques and possible extensions of the method are pointed out.